J. Fluid Mech. (1985), *vol.* 151, *pp.* 367–390
Printed in Great Britain

Scale effects on cavitation inception in submerged water jets: a new look

By K. K. OOI
ABLE Corporation, Anaheim, California 92806

(Received 23 August 1983 and in revised form 6 September 1984)

The present work is an investigation into the scale effects on cavitation inception in submerged water jets. Three scale effects were studied: (i) jet size, (ii) jet velocity and (iii) the nuclei population as a function of dissolved air content in the jet. Holography and schlieren photography were utilized to observe the flow. The results obtained in the present work were then used to illustrate the importance of previously overlooked flow variables in scaling cavitation inception data. An interesting finding of the present investigation was that the cavities at inception did not occur in the cores of the large vortex structures within the shear layer of the jets, as is commonly believed. A new parameter called the 'probable cavitation occurrence' parameter is also introduced in this paper. This parameter incorporates the effects of the nuclei number-density function and peak pressure fluctuations and it shows great promise in scaling cavitation-inception data.

1. Introduction

A thorough and careful survey on published literatures on cavitation inception studies in liquid jets, primarily water jets, has revealed that this area of investigation is in a state of disarray. In the scores of work reported to date, for example, Lienhard & Stephenson (1966), Baker, Holl & Arndt (1975), Arndt & George (1978) and Arndt (1981), there is in general little agreement in the test results and no clear trend is evident. This has continued to puzzle investigators. We strongly believe that the discrepancies in the test results are caused by several less obvious but nevertheless important aspects of the flow that have been often ignored. For instance, there has been no careful documentation of where the cavities are first seen when cavitation inception occurs. Since there are different flow regimes in a jet which are governed by different scaling laws, information on the locations of these cavities could be the key to the correct scaling of the test results. In addition, bubble dynamics prescribe that the susceptibility of a jet to cavitation inception is dependent not only on the number and size of the cavitation nuclei but also on the instantaneous pressure field in the jet under investigation. This implies that a knowledge of the nuclei distribution and the temporal peak pressure fluctuations are required for a complete analysis of the experimental results. Unfortunately, data on such measurements in jets are sorely lacking. It is also equally important to look into certain features of the flow, such as the exit condition of the jet and the spread rate, as these may provide insights into the initial vortex roll-up and the size of the coherent structures, which could in turn affect the cavitation-inception process. This means that, in order to have a better understanding of the scale effects and scaling laws governing cavitation in jets, one must look into the fluid dynamics of the flow as well.

The primary aims of this paper are to demonstrate the importance of some of these

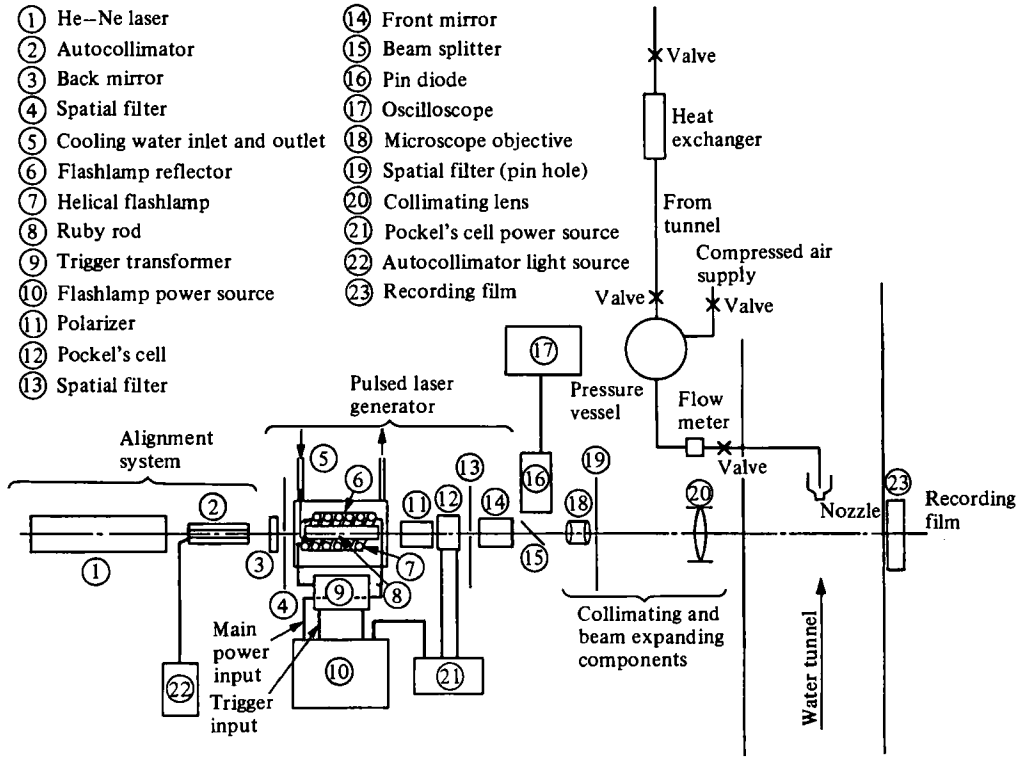

FIGURE 1. Diagram showing the layout of the experimental apparatus.

previously overlooked flow variables and to introduce a new scaling parameter. To accomplish this, cavitation-inception studies were carried out on three different sized submerged axisymmetric water jets. The jets were operated over a range of velocities and at different dissolved air contents. The flow was observed by stroboscopic lighting as well as by schlieren photography and holography at every test condition. Holography was also used to determine the nuclei population in the various regions of the jet. A new method utilizing specially tailored air bubbles was devised to probe the static pressure fluctuations within the jet. A brief description of the test procedures and apparatus follows.

2. Description

2.1. *Test apparatus*

A diagrammatic layout of the experimental apparatus is shown in figure 1. The water tunnel depicted is the Low Turbulence Water Tunnel (LTWT) of Caltech. It was chosen primarily because it represented a test setup wherein a jet of water could be discharged and made to cavitate under prescribed conditions. In addition it provided a reservoir of water which would be treated to meet the test requirements, for example deaerating the water to the desired air content. An environment also exists where the flow could be easily observed. In the present work, the jet was created by discharging tunnel water itself from a pressure vessel through a nozzle assembly into the centreline of the stationary LTWT. A diagram showing the geometrical details of the nozzle assembly is shown in figure 2. Contoured nozzles of different

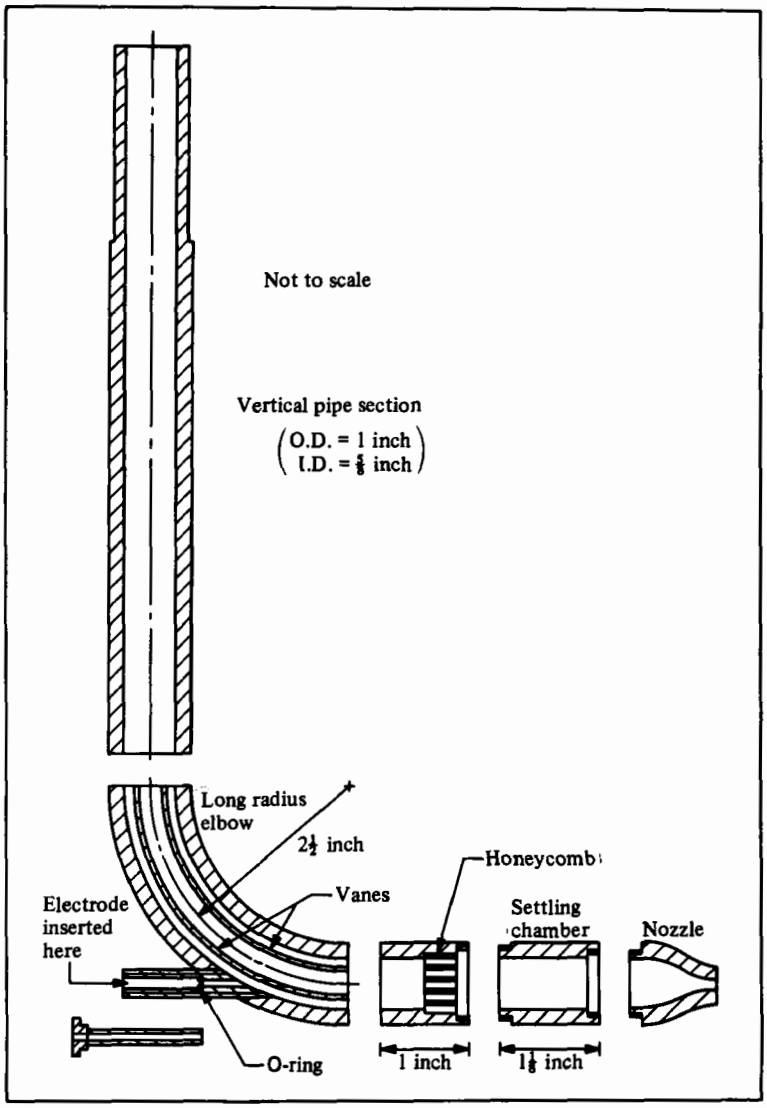

FIGURE 2. Diagram showing the geometrical details of the nozzle assembly.

sizes could be attached to the downstream end of the assembly and in the present investigation nozzles of 3.17, 4.76 and 6.35 mm exit diameters were used.

The flow was observed with the aid of an in-line holocamera, a detailed description of which is found in Katz (1979) and Ooi (1981). The principles governing this holographic technique are discussed in many texts on modern optics, for example Collier, Burkhardt & Lin (1971), and will not be dealt with in detail here. In essence a single collimated laser beam is used to illuminate the test volume. A portion of this beam is then diffracted by the microscopic nuclei present in the test volume and interferes with the remaining undisturbed portion of the beam. This results in an interference pattern which is recorded on high-resolution film. The hologram thus obtained is developed, then placed on the reconstruction system (see Katz 1981) to reproduce a three-dimensional image of the original test region and subsequently

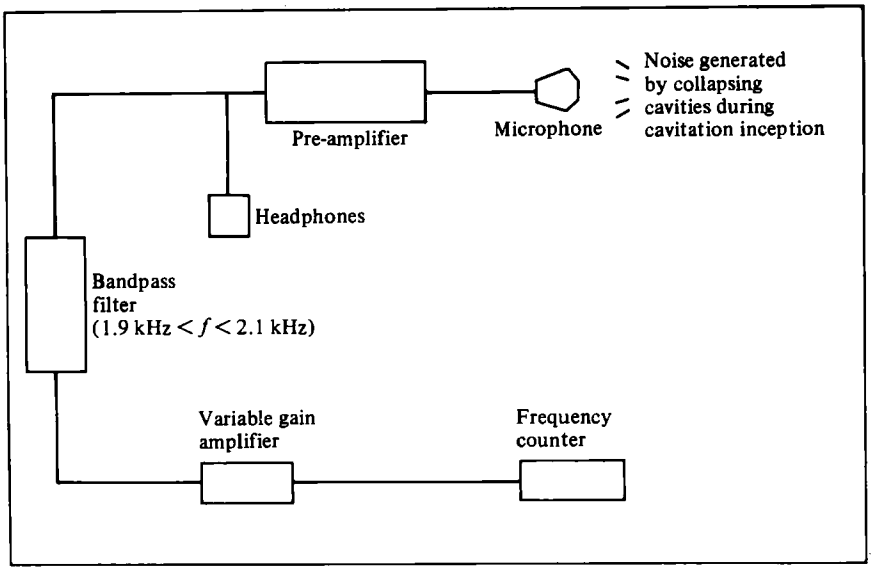

FIGURE 3. Schematic drawing of the cavitation-inception detection system.

analysed. Although only the holographic setup is shown in figure 1, a schlieren system was also employed. This system was described by Gates (1977) and the required 'schlieren effect' in the present work was obtained by heating the jet water to about 2–4 °C above the temperature of the surrounding liquid. Photographs of 'Epsom' salt solution jets (0.5 % concentration by weight) were also taken when high contrast was desired.

Cavitation inception in the jet was detected acoustically by counting the number of cavitation events. The detection system is illustrated in figure 3.

2.2. *Test procedures and measurement techniques*

Some water from the water tunnel was pumped into a pressure vessel and pressurization of the vessel was achieved with the house compressed-air supply. The inlet pressure to this vessel was regulated with a pressure regulator. A jet of water was then discharged into the stationary tunnel at an ambient pressure of 0.9 atm. The pressure in the tunnel was then quickly lowered until cavitation in the jet occurred. The inception point was defined as the instant five or more cavitation events per second were detected by the detection system. The pressure in the tunnel and the exit velocity of the jet at inception were noted. From these measurements, the incipient cavitation index σ_i was calculated from the expression

$$\sigma_i = \frac{P_T - P_v}{\frac{1}{2}\rho V_j^2} \tag{1}$$

where $P_T \equiv$ mean static pressure in the water tunnel at inception,

$P_v \equiv$ vapour pressure of water at the bulk temperature,

$\rho \equiv$ density of water at the bulk temperature,

$V_j \equiv$ exit velocity of the jet.

Between runs, the pressure in the tunnel was raised to its initial value and allowed to sit at that pressure for about 30 s before the next set of data was collected.

The above tests were repeated over a range of jet velocities. Different velocities in the jet were realized through pressurization of the vessel to different pressures and not by throttling of the flow. The tests were also performed sequentially with tunnel water at dissolved air contents of about 14.1, 10.9, 7.7 and 4.2 p.p.m. for each nozzle size. The dissolved-air content in the water was measured with a Van Slyke Blood Analyzer. The incipient cavitation index corresponding to a particular flow condition was obtained by averaging the results of 10 similar runs.

Besides the incipient cavitation index measurements, the flow as the jet was brought to the onset of cavitation and beyond was also observed under stroboscopic light. In addition, schlieren photography and holography were used to give permanent records of the flow conditions which were later analysed.

A new technique was also devised to measure the pressure fluctuations in the present jets. This method relies on the fact that when a bubble is subjected to a fluctuating pressure field it will change in volume accordingly. The magnitude of the pressure fluctuation can then be calculated from this change in bubble size from some chosen referenced bubble volume. In the present work, the change in bubble size was determined from holographic records of the jet when it was seeded with specially tailored air bubbles. The technique allows an instantaneous three-dimensional mapping of the pressure field in the jet. A complete discussion and justification of the method, including the special conditions under which the air bubbles could be employed as static pressure indicators, are found in Ooi & Acosta (1983).

3. Presentation and discussion of results

3.1. *Effect of air content and nuclei population on cavitation inception*

The effects of the dissolved-air content on the inception index for the 3.17, 4.76 and 6.35 mm jets are shown in figures 4–6 respectively. It can be deduced from these plots that for a particular nozzle size and at a fixed air content α the incipient index is independent of the jet Reynolds number. For convenience the experimental results are summarized in table 1. The results displayed in this table clearly demonstrate that the incipient index decreases with decreasing air content for a jet of constant size. Although it has long been speculated that the suppression of the inception point with decreasing air content for flows around an axisymmetric body is due to the reduction of cavitation nuclei, it has only recently been documented quantitatively (e.g. Gates *et al.* 1979; Billet & Gates 1981). The present work represents the first such documentation concerning jets. The nuclei measurements were made in the various regions of the jet at different dissolved air contents, shown schematically in figure 7. These measurements were in the size ranges shown in table 2 and were reduced to a number density $N(\bar{R})$, defined by Gates (1977) and Ooi & Katz (1980), as:

$$N(\bar{R}) = \frac{\text{number of nuclei per unit volume with radii between } R_1 \text{ and } R_2}{R_2 - R_1},$$

where $\bar{R} = \frac{1}{2}(R_2 + R_1)$, and R_1 and R_2 respectively correspond to the lower and upper limits of a certain bubble-size category. The results indicate that when the air content is reduced from 14.3 to 4.2 p.p.m. the nuclei population density is reduced by a factor of approximately 35. No nucleus bigger than 20 μm radius was ever detected.

It can also be seen from table 2 that the nuclei population density is higher in regions outside the jet (regions 2 and 4 of figure 7) than those inside it. This may seem a little

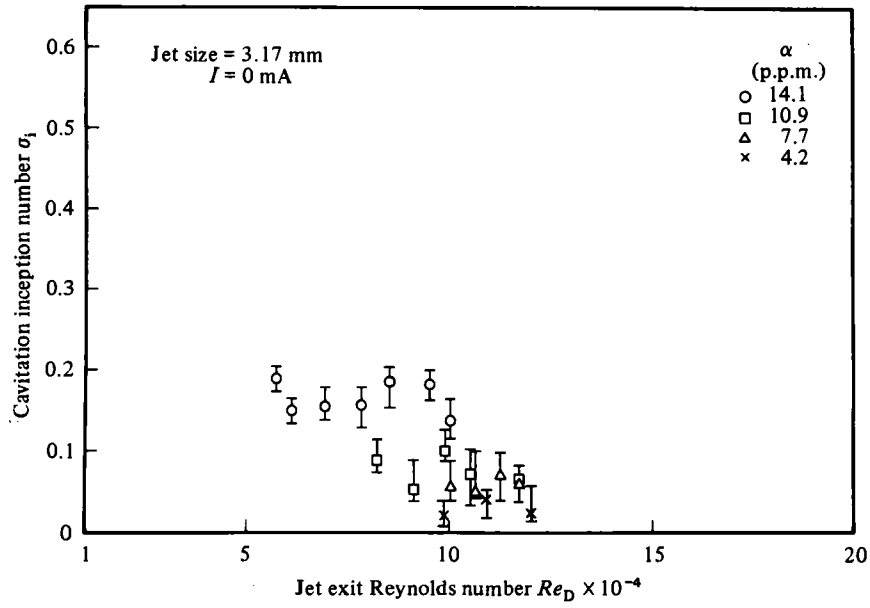

FIGURE 4. Summary of the variation of the incipient cavitation index with Reynolds number at different dissolved-air contents for the 3.17 mm jet.

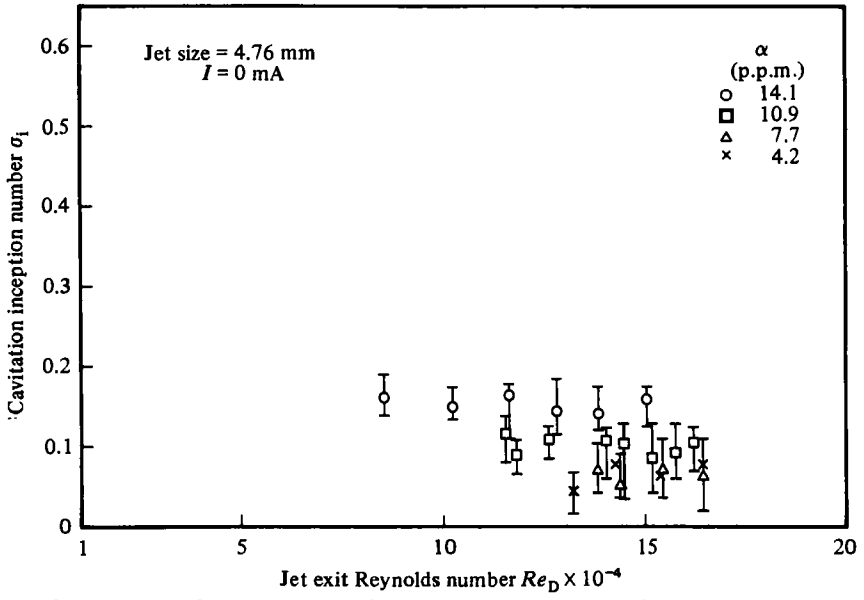

FIGURE 5. Summary of the variation of the incipient cavitation index with Reynolds number at different dissolved-air contents for the 4.76 mm jet.

puzzling at first, but as mentioned earlier the jet in the present studies was created by discharging a column of water from a pressurized vessel. Hence it is to be expected that some of the gas bubbles in the jet were forced into solution by the pressurization process. Consequently the nuclei population density near the jet exit (region 1) would be lower than in the entrainment zone (region 2). It would also be expected that the

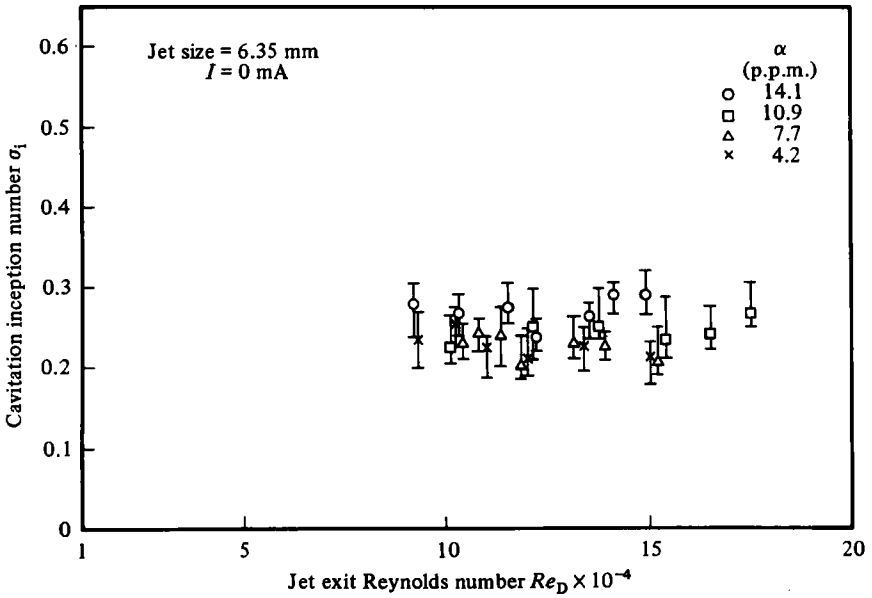

FIGURE 6. Summary of the variation of the incipient cavitation index with Reynolds number at different dissolved-air contents for the 6.35 mm jet.

Size of jet (mm)	Dissolved air content (p.p.m.) 14.1	10.9	7.7	4.2	Comments	Contraction ratio of nozzle
	Measured value of incipient cavitation					
3.17	0.16	0.08	0.06	0.03	Independent	25.00
4.76	0.15	0.11	0.07	0.06	of jet exit	11.11
6.35	0.27	0.24	0.23	0.22	Reynolds number	6.25

TABLE 1. Summary of the measured cavitation indices for the unseeded jet

nuclei density would increase with downstream distance from the nozzle lip because of flow entrainment from the surrounding fluid which contained a higher nuclei population. This can be shown to be the case by comparing the nuclei population density in region 3 with region 1. Also, at a fixed air content, it was found that the population density was independent of the cavitation index and jet size at least up to the cavitation inception point. It is believed that this finding is not universally true but is a consequence of the test procedures adopted. The jet was discharged into a stationary water tunnel sitting at an absolute pressure of 0.9 atm and made to cavitate by rapidly lowering the pressure in the tunnel. Since the duration of a typical run was less than ten seconds, it was fair to assume that the pressure-reduction process itself would not significantly affect the nuclei distribution. It was concluded that the nuclei distribution at a particular air content under the current test procedure was determined by the steady-state condition in the water tunnel, namely the pressure at which the tunnel was kept prior to a test run. This conclusion was reached after the results from an earlier work on the same test setup but with a different test procedure (see Ooi & Katz 1980) gave a nuclei distribution that is distinctly different. Thus it is not difficult to infer that the dissolved-air content in the test fluid is not

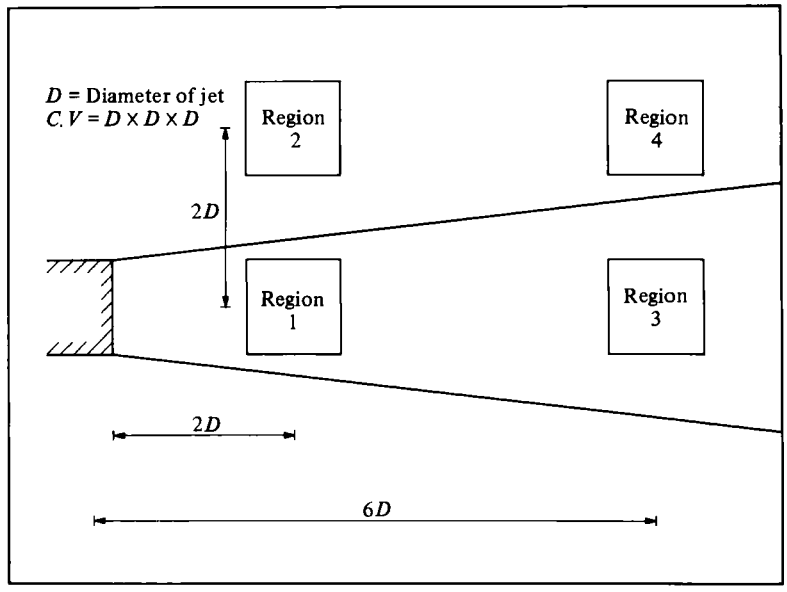

FIGURE 7. A schematic drawing depicting the 4 regions in the jet where nuclei counts were carried out.

	Region 1 $N(\bar{R})$ (m^{-4})		Region 2 $N(\bar{R})$ (m^{-4})		Region 3 $N(\bar{R})$ (m^{-4})		Region 4 $N(\bar{R})$ (m^{-4})	
α (p.p.m.)	(A)	(B)	(A)	(B)	(A)	(B)	(A)	(B)
14.3	3.04×10^{13}	2.48×10^{12}	4.39×10^{13}	2.85×10^{12}	3.41×10^{13}	2.72×10^{12}	4.26×10^{13}	3.02×10^{12}
11.0	1.48×10^{13}	1.46×10^{12}	1.99×10^{13}	1.62×10^{12}	1.35×10^{13}	1.64×10^{12}	1.62×10^{13}	1.62×10^{12}
7.7	4.81×10^{12}	8.21×10^{11}	5.58×10^{12}	9.53×10^{11}	4.30×10^{12}	7.89×10^{11}	4.73×10^{12}	7.03×10^{11}
4.2	1.06×10^{12}	2.14×10^{11}	1.12×10^{12}	2.95×10^{11}	1.07×10^{12}	2.00×10^{11}	1.12×10^{12}	3.18×10^{11}

TABLE 2. Summary of the number density function of nuclei measurements in jets. $A \equiv 5\ \mu m < R \leqslant 10\ \mu m$, $B \equiv 10\ \mu m < R \leqslant 20\ \mu m$.

the sole factor that determines the nuclei distribution, but the adopted test procedures do play an important role.

Table 1 shows that the measured incipient indices for the two smaller jets at the same air content do not differ greatly from each other. On the other hand, the largest jet exhibits an inception index that is substantially different from the other two. It can be demonstrated that the cause could be the different nuclei population in the region that is susceptible to cavitation inception in the jet. As a direct consequence of extensive flow visualization, it has been found that, for the two smaller jets, cavitation inception occurred in a region beyond the potential core of the jet and not in the shear layer within the flow-establishment zone. These cavities were seen to be confined to a region between 6 and 16 diameters downstream of the jet exit but favouring no particular radial position. However, in the biggest jet, cavities have been observed in the shear layer as well as beyond the potential core during cavitation inception. But at no time were any cavities detected less than two jet diameters downstream of the nozzle lip or beyond fourteen jet diameters. Typical examples of

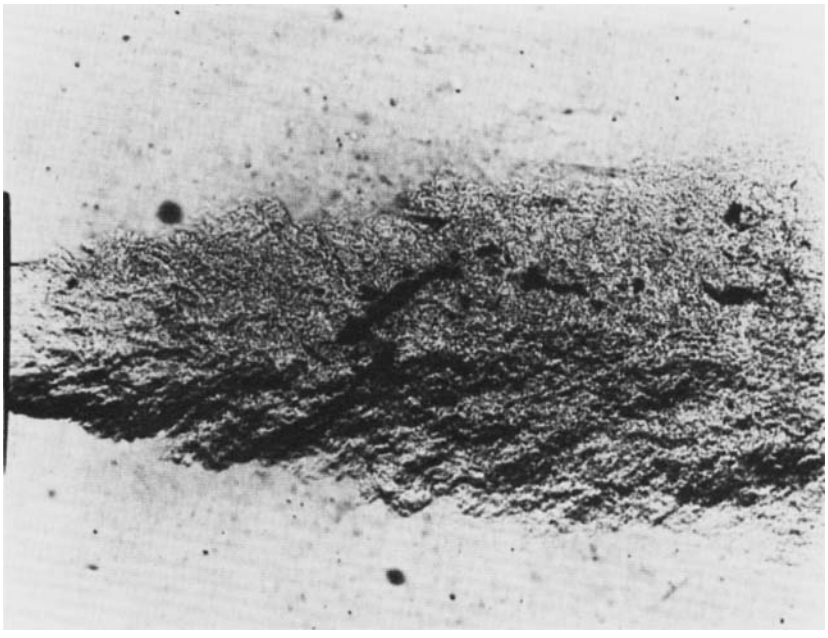

FIGURE 8. Schlieren photograph of cavitation inception in the 6.35 mm diameter jet at $Re_D = 1.63 \times 10^5$ and $\sigma_i = 0.25$. The dissolved-air content is 14.1 p.p.m.

cavitation inception in jets are shown in figures 8–10; the cavities appear as dark irregular shaped patches within the jets in the photographs.

The widths of the jets as a function of jet position were measured directly from the schlieren photographs and these results are summarized graphically in figures 11 (*a–c*). With the combined information on the widths of the jets and the observed extent of the region that is susceptible to cavitation inception discussed above, it has been estimated that the volume of the cavitation-prone regions of the 6.35, 4.76 and 3.17 mm jets were respectively 50.3, 12.5 and 5.41 cm^3. Since the nuclei density at a fixed air content has been found to be independent of jet size, it followed that the calculated volumes were also direct ratios of the number of nuclei in the cavitation-prone regimes of the three jets. Consequently it should be apparent that the degree of susceptibility of a jet to cavitation inception was governed by the number of nuclei present in the cavitation-prone region at any instant.

If this nuclei population was the only determining parameter, then one would expect the measured cavitation index σ_i to be scaled up or down in the same proportion when the nuclei population was altered as a result of a different dissolved-air content in the water. However, it was evident from the present measurements that this was not the case; the effect of a change in the number of nuclei on the cavitation inception number was more pronounced on the 3.17 and 4.76 mm jets than for the 6.35 mm jet. This implied that at least one other scaling parameter was involved. The most likely candidate was the intensity of the pressure fluctuation since this was responsible for initiating cavitation.

3.2. *Effect of fluctuating pressure intensity*

Using the bubble-injection technique described by Ooi & Acosta (1983), it has been discovered that a whole spectrum of peak pressure fluctuation intensities exists at

FIGURE 9. Schlieren photograph of cavitation inception in the 4.76 mm diameter jet at $Re_D = 1.40 \times 10^5$ and $\sigma_i = 0.16$. The dissolved-air content is 14.1 p.p.m.

FIGURE 10. Schlieren photograph of cavitation inception in the 3.17 mm diameter jet at $Re_D = 1.02 \times 10^5$ and $\sigma_i = 0.15$. The dissolved-air content is 14.1 p.p.m.

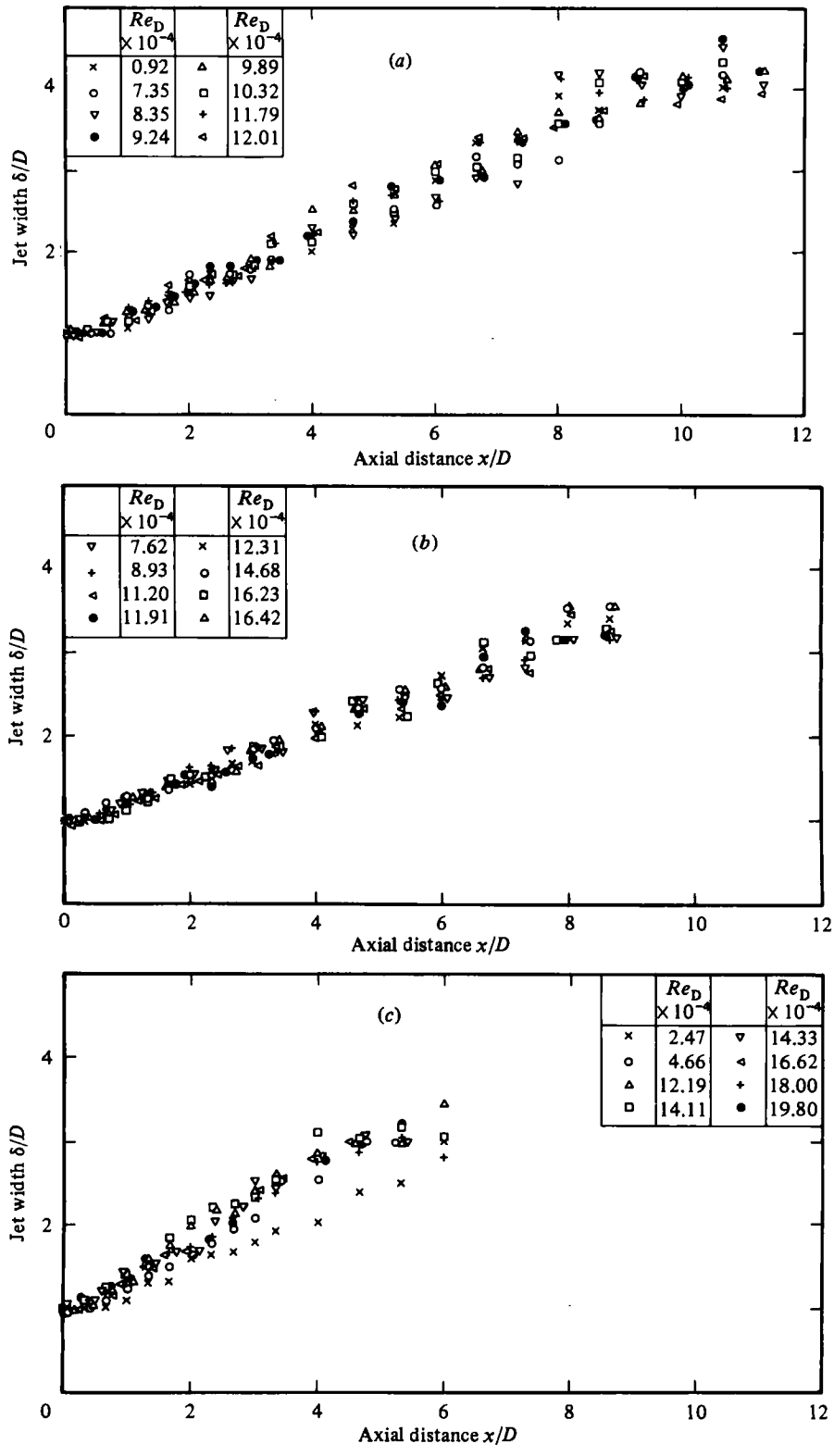

FIGURE 11. Plots of the non-dimensional jet width δ/D versus the dimensionless axial position for the (*a*) 3.17 mm jet, (*b*) 4.76 mm jet, and (*c*) 6.35 mm jet.

any one instant in the jet. This finding is consistent with that of Arndt & George (1978). In our measurements, negative peak pressure fluctuations ranging from 0 to 160 % of the dynamic head at jet exit were detected. However, this is not to say that inception occurred at the very first negative pressure fluctuation experienced by a nucleus. Two conditions have to be satisfied for inception to occur. First, the pressure fluctuation must be intense enough to create a local pressure that is conducive to the explosive growth of a cavitation nucleus. It has been shown from bubble dynamics by Knapp & Hammitt (1970) and Arndt & George (1978) that this local pressure P_1 is reached when

$$P_1 = P_v - \frac{4S}{3R}, \tag{2}$$

where $S \equiv$ surface tension force per unit length,

$R \equiv$ instantaneous bubble radius.

The second condition to be met is that the local pressure described in (2) must persist at, or even below, that value for a period of time that is long in comparison to the response time of the bubble or nucleus. It has already been reported that no nucleus greater than 20 μm in radius was ever detected in the present jets. Calculations show that a bubble of this size has a response time of the order of ten microseconds. In addition, based on the investigations of Michalke & Fuchs (1975) and Lau, Fischer & Fuchs (1972), it has been estimated that the timescale of the pressure fluctuations in the present jets are of the order of a hundred microseconds or more. Since the response time of the bubble is at least an order of magnitude less than the pressure-fluctuation timescale or the traverse time across the cavitation-prone region of the jet, it can be deduced that cavitation inception will occur once (2) is satisfied. This deduction is confirmed by holograms of the jets at conditions approaching cavitation inception which showed that the sizes of the nuclei were no bigger than those at conditions far removed from the inception point. This suggests that inception occurred the very instant the nucleus sensed the pressure conducive to its explosive growth. For the present discussion the traverse time is defined as the elapsed time between the instants the nucleus enters and leaves the cavitation-prone region of the jet. The order of magnitude of the traverse time is estimated by dividing the axial extent of the cavitation-prone region with a representative velocity in that region.

It has been observed that the mean static pressure in the jet when cavitation inception was declared, was a function of numerous variables, for example the velocity and size of the jet. This meant that different minimum magnitudes of negative peak pressure fluctuations were required to initiate cavitation in each case. Pressure measurements made in the 3.17 mm jet and reported by Ooi (1981) showed that the different pressure fluctuation intensities considered above have different probabilities of occurring. An example of the probability density curve is presented in figure 12. Consequently, the cumulative probability of favourable pressure fluctuation was also different from one flow condition to another (a favourable pressure fluctuation being defined as any fluctuation that brought about a local pressure that was at least as low as that required for cavitation inception). For ease of reference, these cumulative probabilities are tabulated in table 3 where P'_D is the ratio of the peak pressure fluctuation to the dynamic head of the jet at exit. It is highly probable that this variable entered as a second scaling parameter for the incipient index.

A new parameter, the probable cavitation occurrence or event parameter N_p, is defined as

$$N_p = nP(P_f), \tag{3}$$

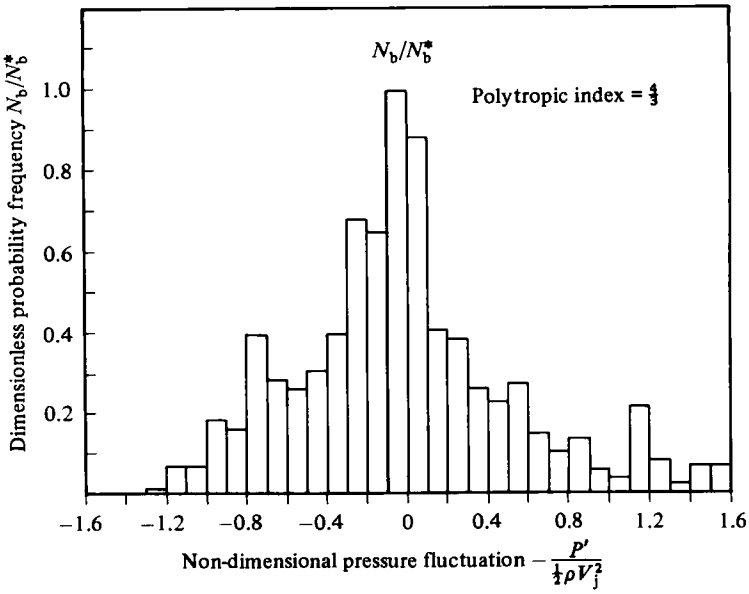

FIGURE 12. Probability histogram showing the distribution of the pressure fluctuation intensities in a jet.

	$P(P_f)$ (%)		$P(P_f)$ (%)
$0 \geqslant P'_D \geqslant -\infty$	55.58	$-0.9 \geqslant P'_D \geqslant -\infty$	4.93
$-0.1 \geqslant P'_D \geqslant -\infty$	43.24	$-1.0 \geqslant P'_D \geqslant -\infty$	3.08
$-0.2 \geqslant P'_D \geqslant -\infty$	33.49	$-1.1 \geqslant P'_D \geqslant -\infty$	1.85
$-0.3 \geqslant P'_D \geqslant -\infty$	26.09	$-1.2 \geqslant P'_D \geqslant -\infty$	0.86
$-0.4 \geqslant P'_D \geqslant -\infty$	20.54	$-1.3 \geqslant P'_D \geqslant -\infty$	0.43
$-0.5 \geqslant P'_D \geqslant -\infty$	16.22	$-1.4 \geqslant P'_D \geqslant -\infty$	0.18
$-0.6 \geqslant P'_D \geqslant -\infty$	12.70	$-1.5 \geqslant P'_D \geqslant -\infty$	0.06
$-0.7 \geqslant P'_D \geqslant -\infty$	9.74	$-1.6 \geqslant P'_D \geqslant -\infty$	0.00
$-0.8 \geqslant P'_D \geqslant -\infty$	7.15		

TABLE 3. A tabulation of the cumulative probabilities of dimensionless negative peak pressure-fluctuation intensities

where n is the total number of nuclei present in the cavitation-prone region of the jet; and $P(P_f)$ is the cumulative probability of favourable negative peak fluctuation intensities that would cause the explosive growth of a cavitation nucleus. In general, nuclei of various sizes are constantly present in the jet. These nuclei are frequently grouped in different size categories to facilitate documentation. In addition to having different population densities, the nuclei in the different categories require different minimum pressure fluctuations to cause them to grow explosively. Consequently the value of N_p as defined in (3) would vary from one size category to another. Hence (3) would be generalized to

$$N_P = \sum_k N_{pk}, \tag{4}$$

where $N_{pk} = n_k P_k(P_f)$. The above symbols have the same meaning as the corresponding symbols without the subscript k, except they now represent the variables at a specific nuclei size category which is characterized by a mean radius. It follows that,

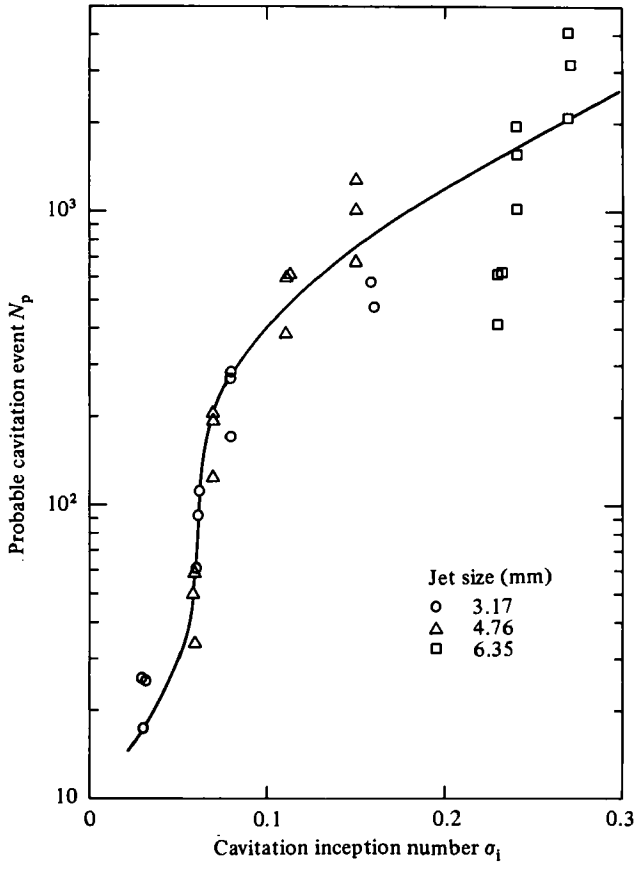

FIGURE 13. A plot of N_p versus σ_i for the 3.17, 4.76 and 6.35 mm jets at different jet exit velocities.

if (4) is an adequate scaling parameter for cavitation inception, then σ_i would be a function of N_p only. The results of the present work were used to ascertain if N_p is a useful scaling parameter.

The values N_p corresponding to the various σ_i values at different dissolved-air contents were computed at jet velocities of 10, 20 and 30 m/s for the three jets. The method by which these values were obtained is described in Ooi (1981) and only the results are discussed here. However, it should be stressed that, since the pressure fluctuation measurements were only conducted in the 3.17 mm jet and at one velocity, two assumptions had to be made to enable the calculations to be extended to the two bigger jets. These assumptions were: (*a*) that the peak pressure fluctuation intensities scaled with the dynamic head of the jet at exit; and (*b*) that the probability distribution curve of the peak pressure fluctuations was the same for all three jets. The calculated results are summarized in figure 13. It can be seen from this plot that the data points, especially those of the 6.35 mm jet, do not all fall on the same curve. It is conceivable that the probability distribution curve of the peak pressure fluctuations is not universal and is a function of the jet size or some yet undefined parameter. Consequently, the computed N_p values for the bigger jets would not be scaled in the right proportion. It would be premature to say that this is the reason for the scatter in the data points without further investigation. Nevertheless, there is a strong indication that σ_i is a function of N_p.

It has been mentioned earlier that, in the present work, inception was said to take place when 5 cavitation events or more per second were detected. It was suggested that it would be more appropriate to scale the count of events to the size of the cavitating region in the jet. Thus in a larger jet inception would be called at a corrrespondingly higher count. The question at this point is whether the measured σ_i values are significantly changed as a result of this new definition of the inception point. Through careful flow observation it is known that once inception occurs the number of cavitation events per second increases very rapidly. This implies that the mean static pressures between the different definitions of the inception points (and consequently σ_i) will not be significantly different, especially for jets with a high nuclei population. This will be shown statistically to be mathematically consistent.

It is to be expected that the probability of occurrence of cavitation events is governed by the number of nuclei in the cavitation-prone region of the jet and the cumulative probability of favourable fluctuations, that is the parameter N_p. Since the occurrence of these events is a Poisson process, the probability of, say, m events occurring per second is described by

$$P(m) = \frac{(n_p)^m \, e^{-N_p}}{m!} \tag{5}$$

and

$$P(\geqslant m) = 1 - \sum_{\phi=1}^{m} P(\phi), \tag{6}$$

where $P(\geqslant m)$ denotes the probability of the occurrence of m events or more per second. As a conservative estimate, N_p will assume a value of 500. It can then be shown from (5) and (6) that the probability of 5 or of 50 events occurring per second is essentially unity, thus indicating that the inception indices in the present investigation are not significantly affected. However, it can also be deduced from the above analysis that, if the value of N_p is small in comparison with the number arbitrarily assigned as the inception point, then the difference in value of the measured σ_i by virtue of this different definition of the inception point will be significant.

3.3. *Effect of jet exit velocity*

One other interesting finding of the present studies is that σ_i for a particular nozzle size is independent of the jet exit Reynolds number, at least over the range of velocities investigated. A possible reason for this finding is discussed below.

Consider the case of a jet of arbitrary size. As mentioned before, inception would only occur when

$$P_i \leqslant P_v - \frac{4S}{3R}. \tag{7}$$

If inception occurred, at a mean pressure denoted by P_T, then the minimum negative pressure fluctuation P' required to initiate cavitation is given by

$$P' = P_i - P_T. \tag{8}$$

Substituting (7) into (8) gives

$$P' = P_v - \frac{4S}{3R} - P_T. \tag{9}$$

Furthermore if $P' = K\frac{1}{2}\rho V_j^2$, where K is a constant, then (9) can be rewritten as

$$K = \frac{P_v - P_T}{\frac{1}{2}\rho V_j^2} - \frac{8S}{3\rho R V_j^2} \tag{10}$$

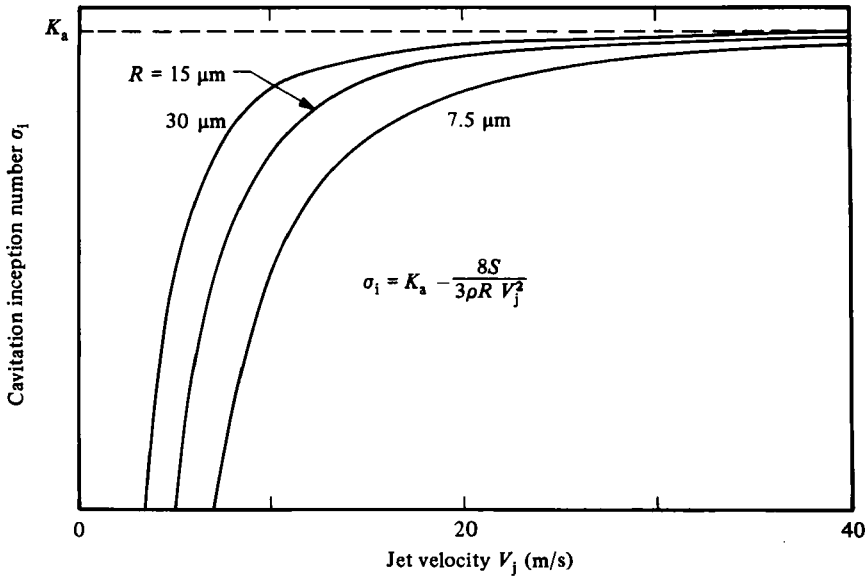

FIGURE 14. A plot of σ_i versus V_j for the equation $\sigma_i = K_a - 8S/3\rho R V_j^2$.

or
$$\sigma_i = K_a - \Delta\sigma_i, \tag{11}$$

where
$$\Delta\sigma_i = \frac{8S}{3\rho R V_j^2}$$

and $K_a = -K$ = scaling constant. For the purpose of this discussion (11) was plotted over the range of nuclei sizes found in the present jets. This is shown in figure 14 for an arbitrary K_a. In the current work, the operating pressure in the water tunnel limited the σ_i measurements to the velocity range of 20–35 m/s. It can be seen from this plot that, over this range of velocities, σ_i is only a weak function of the jet velocity, and the maximum change in the value of $\Delta\sigma_i$ is approximately 0.05. This change in value of $\Delta\sigma_i$ with velocity is of the same order of magnitude as the scatter in the measured σ_i. Consequently, the variation of $\Delta\sigma_i$ with velocity is masked and thus gives the appearance that the incipient index is independent of Reynolds number at a constant jet size. It is also apparent from figure 14 that, if the jet had been operated at velocities considerably lower than 20 m/s, then σ_i would definitely show a dependence on Reynolds number, for a constant jet size. This was found to be the case by Ooi (1981). Since K_a is arbitrary, the above explanation holds for all three jets.

If K_a had indeed been independent of jet size as assumed, then (11) says that the measured values of σ_i for all the jets at the same velocity would be the same, since the jets have identical nuclei size distribution. However, the measured σ_i are different, thus suggesting that K_a could possibly be a function of jet size or perhaps some unknown parameter. It should be emphasized that all the above arguments are only valid if K_a scaled as the dynamic head of the jet at exit. Unfortunately this information is at present unavailable, bearing in mind that K_a is a 'scaling constant' for the peak and not the r.m.s. pressure fluctuations.

The results of the present studies, as well as those of others, have shown that, at a high dissolved-air content, inception occurs at a relatively high mean pressure in the jet. In such a situation, only a few locations in the jet experienced local pressure fluctuations that were intense enough to cause cavitation. As a result, cavities at

inception only appeared in these few positions. However, at a low air content, the mean pressure at inception was considerably lower, which resulted in many locations having local pressures that were conducive to the explosive growth of the nuclei. Thus the cavities were much more extensive than in the former case as is evident in figure 15 (*a–c*).

3.4. *Coherent structures*

Another important aspect of jet flow which has received little attention in cavitation studies until very recently is the large coherent structures. The existence of these structures was first reported by Brown & Roshko (1974) and since then others, including Davies & Yule (1975) and Perry & Watmuff (1981), have further established their presence. In the present work, these coherent structures could only be observed up to a relatively low Reynolds number (based on axial position) of approximately 45000. An example of the structures is shown in figure 16. Unlike the structures in the plane shear layer described by Brown & Roshko (1974) the present large-scale structures only remained distinct up to the second or third vortices. Beyond that the flow became three-dimensional with a multitude of small grainy structures. It is also apparent from figure 17 (*a–d*) that the cellular structures are located just downstream of the laminar region of the jet. These structures were also observed by Konrad (1976). It is believed that they begin as hairpin vortices which later become unstable and break up to give the three-dimensional small-scale structures in the jet as they proceed downstream. Notice also that the laminar region of the jet retreats towards the nozzle lip as the jet velocity is increased. At the same time the scale of the cellular structures continues to be reduced.

As a consequence of the work of Brown & Roshko and others, it is now generally believed that the longitudinal increase in the scale of the large eddy structures, and therefore the spreading rate of the shear layer, is accomplished by the coalescence of two or more of the neighbouring structures. Thus any factors that affect the scale of these structures would affect directly the spread rate and consequently the size of the cavitation-prone region in the jet. In the work of Brown & Roshko, the estimated slope of the spread of the plane shear layer was 0.38. In the present jets, slopes of 0.35, 0.33 and 0.43 were obtained respectively for the 3.17, 4.76 and 6.35 mm jets. The reason for the relatively large difference in spread rates between the two smaller jets and the largest jet is presently unclear.

3.5. *Probable causes for discrepancies in test results*

There is a discrepancy between the present results and those of Lienhard & Stephenson (1966) as summarized in table 4. It is believed that this discrepancy in findings is caused by the different nuclei populations in the jets that are the results of different test procedures. Furthermore it has been reported by Hussain & Zedan (1978) that the nature and thickness of the boundary layer upstream of the nozzle exit has a significant effect on the development of a jet. Since the boundary layers between the present jets and those of Lienhard & Stephenson may be substantially different, it is conceivable that this may result in differences of pressure fluctuation peaks and therefore cavitation inception data.

Before ending this discussion, it should be noted that, contrary to the suggestion of Sami, Carmody & Rouse (1967), the cavities at inception do not occur in the cores of the large vortices in the shear layer of the jets. Careful studies of hundreds of photographs and holograms of the present jets at inception have clearly shown that the cavities always appear in the distance range stated earlier but favouring no

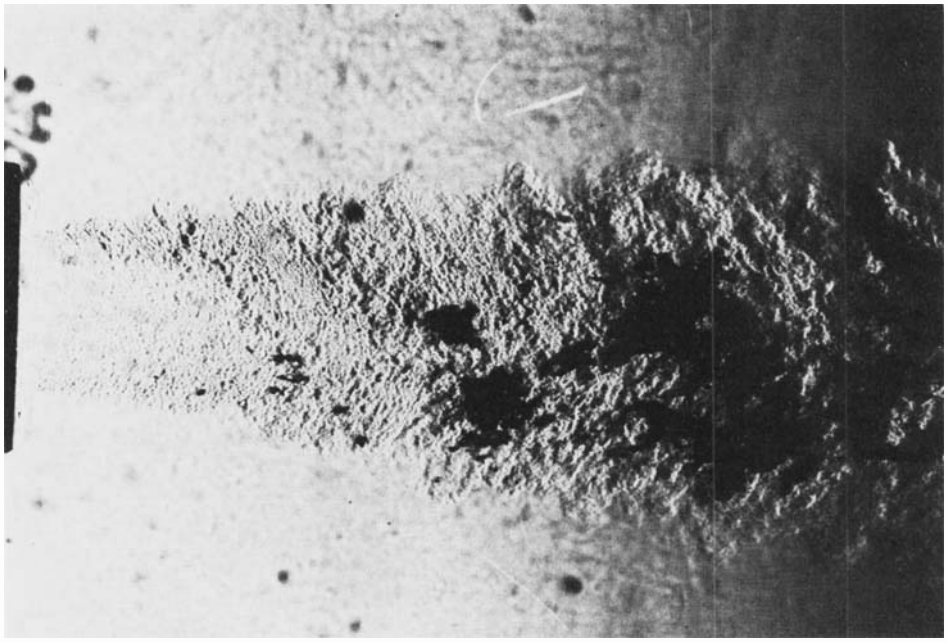

(*a*)

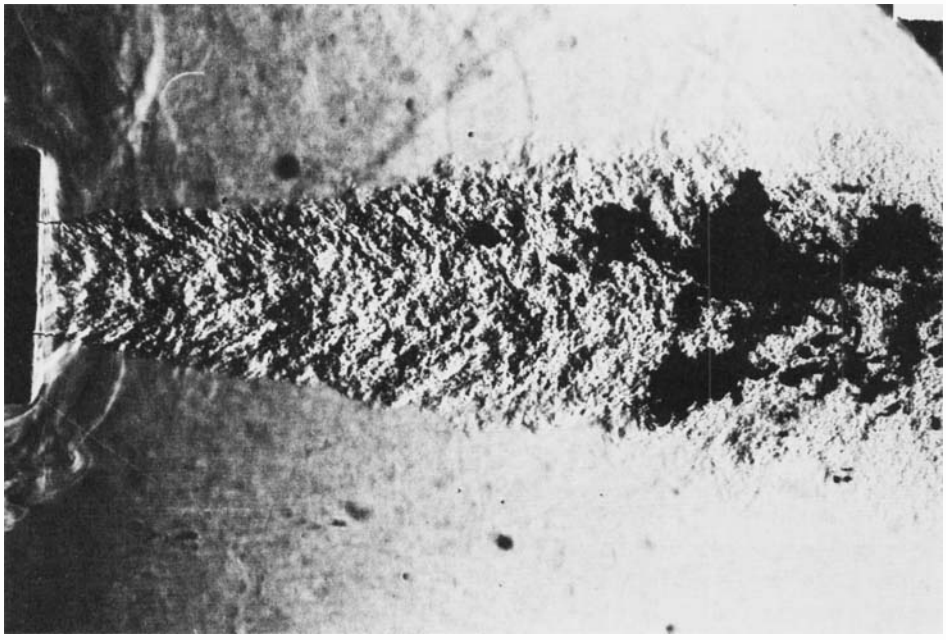

(*b*)

FIGURE 15*a*,*b*. For caption see facing page.

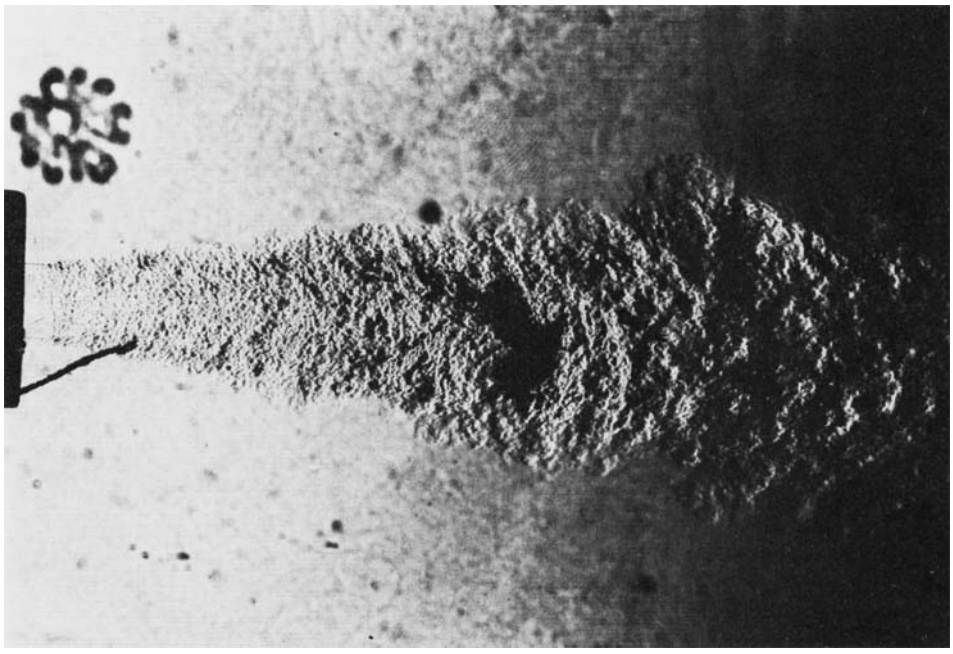

(*c*)

FIGURE 15. Schlieren photographs of cavitation inception in (*a*) 6.35 mm jet at $Re_D = 2.06 \times 10^5$ and $\sigma_i = 0.22$, (*b*) 4.76 mm jet at $Re_D = 1.47 \times 10^5$ and $\sigma_i = 0.09$, (*c*) 3.17 mm jet at $Re_D = 8.35 \times 10^4$ and $\sigma_i = 0.08$. The dissolved-air content is 7.7 p.p.m.

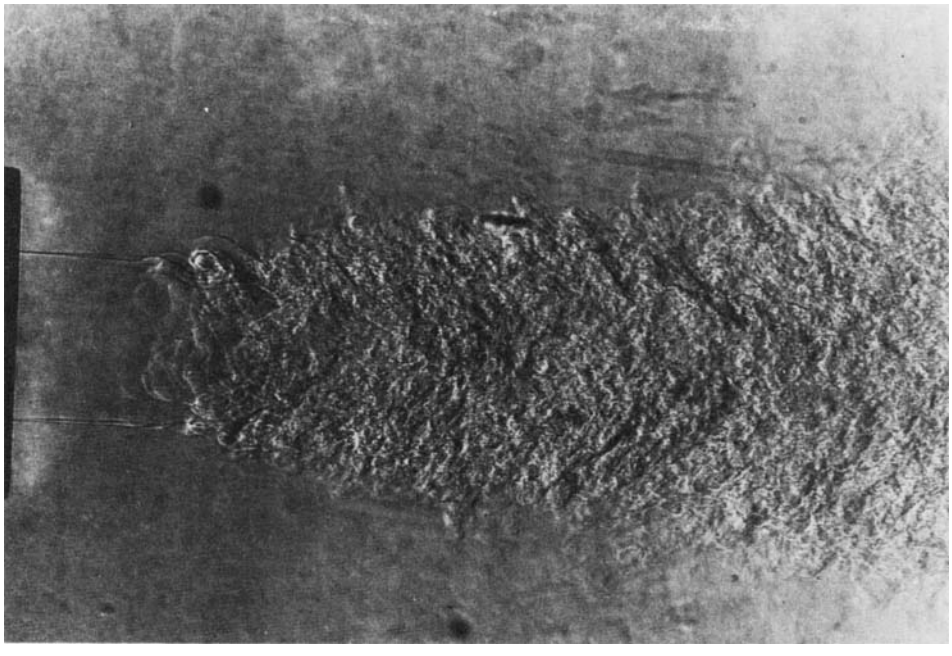

FIGURE 16. Schlieren photograph showing the large eddies in the 6.35 mm jet at $Re_D = 3.1 \times 10^4$.

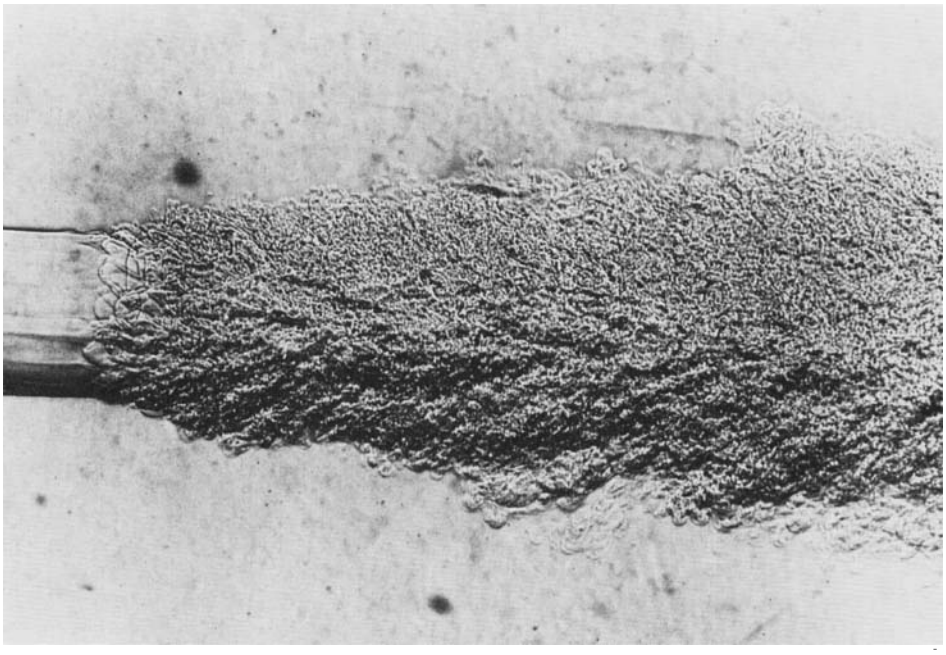

(a)

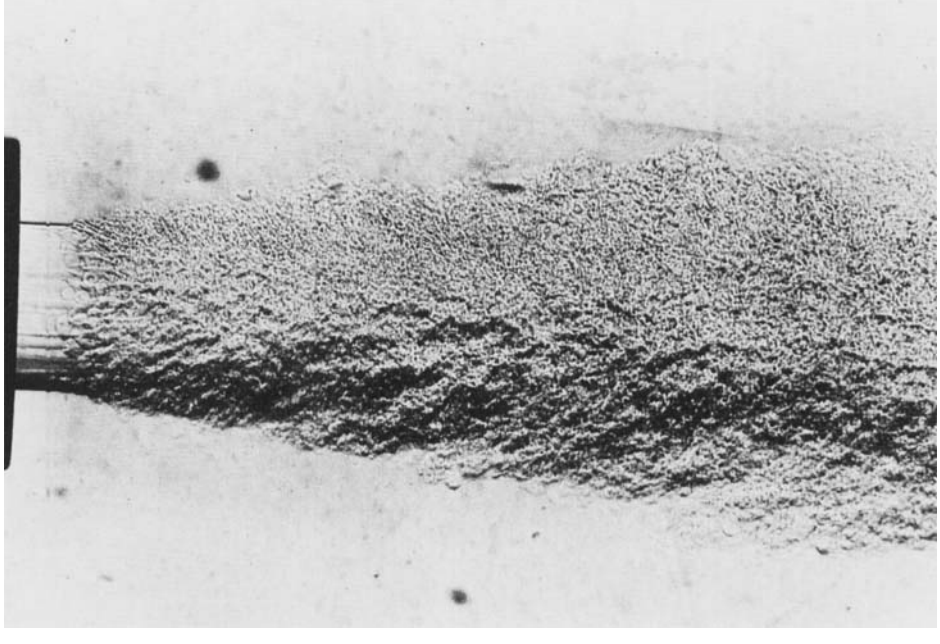

(b)

FIGURE 17a,b. For caption see facing page.

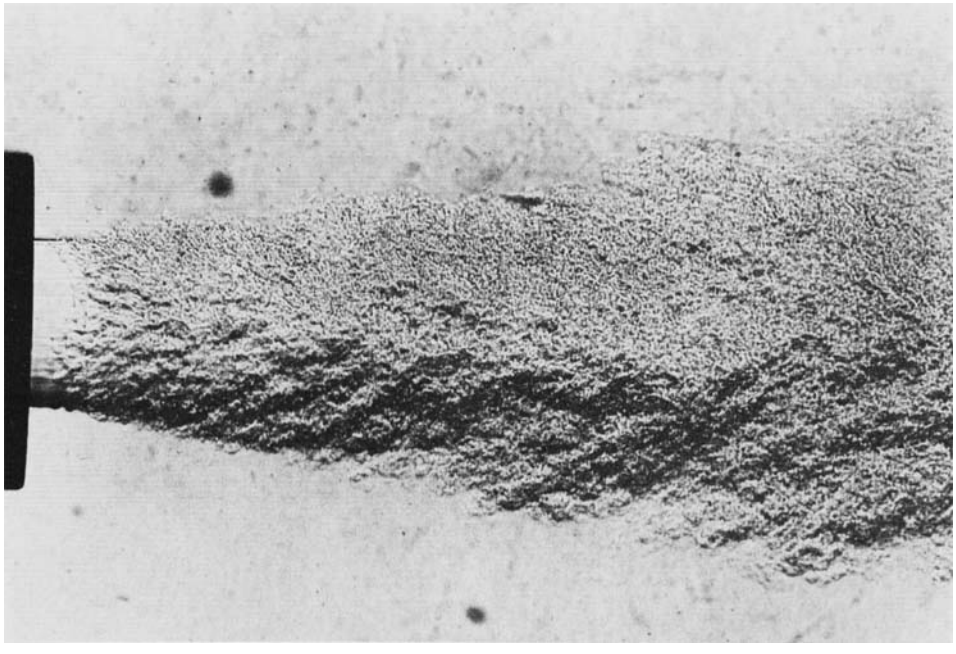

(*c*)

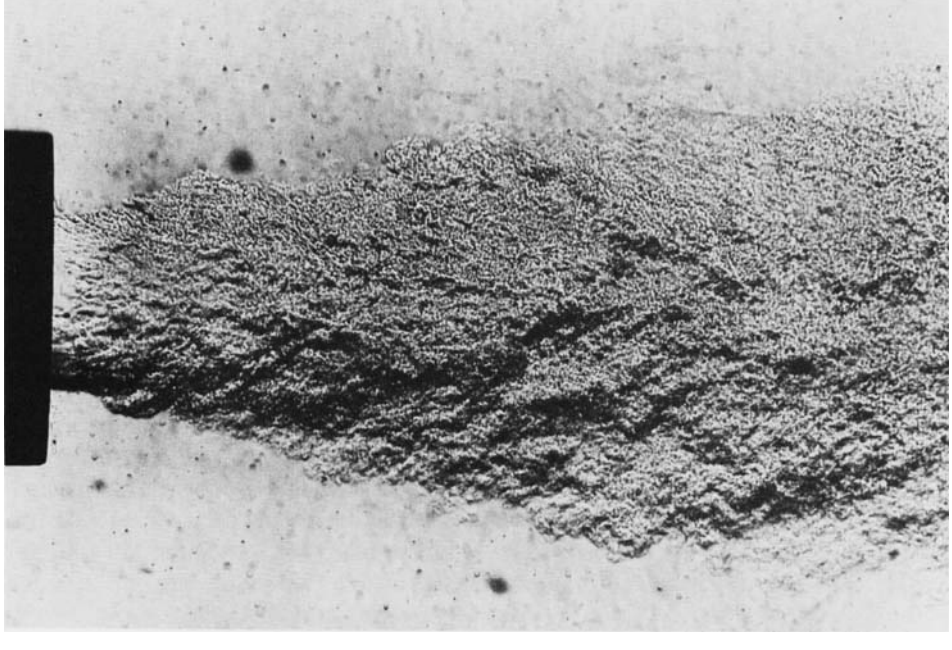

(*d*)

FIGURE 17. Schlieren photographs of the non-cavitating 6.35 mm jet taken with knife edge parallel to the flow direction: (*a*) $Re_D = 3.03 \times 10^4$, (*b*) 7.20×10^4, (*c*) 1.00×10^5, (*d*) 1.57×10^5.

Investigator	Incipient index 6.35 mm jet	3.17 mm jet	Air content
Present work	0.27	0.16	14 p.p.m.
Lienhard & Stephenson (1966)	0.55	0.25	Not measured, probably near saturation, i.e. around 14 p.p.m.

TABLE 4. A comparison of inception data

FIGURE 18. Schlieren photograph showing cavitation inception in the core of a vortex.

particular radial position within the three-dimensional small-scale grainy structures. Only in one photograph was inception detected in the core of a large-scale eddy in the shear layer. This is shown in figure 18.

It was also mentioned earlier that cavitation inception always starts in the region beyond the potential core for the two smaller jets. For the 6.35 mm jet, cavities have been seen in both the shear layers as well as in the region where the shear layers have already merged. In addition, Arndt (1981) has reported that, for a 25.4 mm jet, cavities at inception are seen only in the shear layers. Collectively, these observations imply that the region in a jet in which the cavities first appear as the jet is made to cavitate is dependent on jet size. More appropriately, it has been postulated by Ooi (1981) that a likely parameter dictating where cavities first appear in a jet is the ratio of the probable cavitation occurrence parameters in the shear layer to that in the region beyond the potential core. Interested readers are requested to refer to Ooi (1981) for a more detailed discussion.

3.6. *Proposals for future studies*

In the discussion, it was suggested that the pressure fluctuation peaks in a jet may be affected by the nature and thickness of the boundary layer upstream of the nozzle exit. A systematic study of these and other parameters on the pressure-fluctuation peaks could provide valuable answers to the questions posed by the present work. Also, the pressure-fluctuation measurements could be extended to cover a range of jet sizes and velocities. The resulting probability distribution curves of peak fluctuation intensities for the various flow configurations would enable the determination of whether the cavitation occurrence parameter N_p as introduced in this paper is a universal scaling constant for inception studies.

4. Conclusions

It has been demonstrated that the spread rate of a jet and the test procedures affect the nuclei distribution and population in a jet. Consequently the past practice of using the dissolved air content as a direct indication of the nuclei distribution should be discouraged. Instead, actual nuclei measurements should be made. It has also been found that the incipient index σ_i appears to be adequately defined by the equation $\sigma_i = K_a - \Delta\sigma_i$, although the exact value and the dependence of K_a on flow variables are unknown at present. In addition, more attempts should be made to measure the peak pressure fluctuations in the jet and not just the r.m.s. values since the former is more useful for cavitation-inception studies. There is also a strong indication that σ_i could be scaled with the newly defined parameter N_p, which is a correlation between the nuclei population in the cavitation-prone region of the jet and the cumulative probability of favourable negative peak fluctuations. Finally, the cavities at inception in the present jets do not occur in the core of the large coherent structures in the shear layer but are scattered randomly within the fine grainy three-dimensional structure of the jet within a defined axial range.

The author is grateful to Professors A. J. Acosta and R. H. Sabersky of the California Institute of Technology for their valuable advice, suggestions, and for the many helpful discussion sessions. Thanks also go to Susan Berkley and Carol Kirsch for undertaking the chores of typing and organizing the paper.

This work was supported by Naval Sea Systems Command General Hydromechanics Research Program administered by the David Taylor Naval Research and Development Center under Contract No. N00014-75-C-0378, which was greatly appreciated.

REFERENCES

ARNDT, R. E. A. 1981 Cavitation in fluid machinery and hydraulic structures. *Ann. Rev. Fluid Mech.* **13**, 273–328.

ARNDT, R. E. A. & GEORGE, W. K. 1978 Pressure fields and cavitation in turbulent shear flows. In *Proc. 12th Symp. Naval Hydrodynamics, Washington, D.C.*, pp. 327–339.

BAKER, C. B., HOLL, J. W. & ARNDT, R. E. A. 1975 The influence of gas content and polyethylene oxide additive upon confined jet cavitation in water. *Appl. Res. Lab., TM* 75-274, *Penn. State Univ.*

BILLET, M. & GATES, E. M. 1981 A comparison of two optical techniques for measuring cavitation nuclei. *Trans. ASME* I: *J. Fluids Engng* **103**, 8–13.

BROWN, G. L. & ROSHKO, A. 1974 On density effects and large structures in turbulent mixing layers. *J. Fluid Mech.* **64**, 775–816.

COLLIER, R. J., BURKHARDT, C. B. & LIN, L. H. 1971 *Optical Holography*. Academic.

DAVIES, P. O. A. L. & YULE, A. J. 1975 Coherent structures in turbulence. *J. Fluid Mech.* **69**, 513–537.

FUCHS, H. V. 1973 Resolution of turbulent jet pressure into azimuthal components. In *Advis. Group Aerosp. Res. and Dev. Conf. Proc.*, No. **131**, Paper 27.

GATES, E. M. 1977 The influence of freestream turbulence, free stream nuclei populations and a drag-reducing polymer on cavitation inception on two axisymmetric bodies. Ph.D dissertation, California Institute of Technology.

GATES, E. M. & ACOSTA, A. J. 1978 Some effects of several freestream factors on cavitation inception of axisymmetric bodies. In *Proc. 12th Symp. Naval Hydrodynamics, Washington, D.C.*, pp. 86–108.

GATES, E. M., BILLET, M. L., KATZ, J., OOI, K. K., HOLL, J. W. & ACOSTA, A. J. 1979 Cavitation inception and nuclei distribution, joint ARL/CIT experiments. *California Institute of Technology, Rep.* E244.1.

HUSSAIN, A. K. M. F. & ZEDAN, M. F. 1978 Effects of the initial condition of the axisymmetric free shear layer: effects of the initial momentum thickness. *Phys. Fluids* **21**, 1100–1112.

KATZ, J. 1979 Construction and calibration of an holograph camera designed for micro bubbles observation in cavitation research. *CIT Engng Rep.* 183–4.

KATZ, J. 1981 Cavitation inception in separated flows. *CIT Engng Rep.* 183–5.

KELLER, A. P. 1972 The influence of the cavitation nucleus spectrum on cavitation inception, investigated with a scattered light counting method. *Trans. ASME* D: *J. Basic Engng* **94**, 917–925.

KNAPP, R. T., DAILY, J. W. & HAMMIT, F. G. 1970 *Cavitation*. McGraw-Hill.

KONRAD, J. H. 1976 An experimental investigation of mixing in two-dimensional turbulent shear flows with applications to diffusion-limited chemical reactions. *Project Squid Tech. Rep.* CIT-8-PU.

LAU, J. C., FISCHER, M. J. & FUCHS, H. V. 1972 The intrinsic structure of turbulent jets. *J. Sound Vib.* **22**, 379–406.

LIENHARD, J. H. & STEPHENSON, J. M. 1966 Temperature and scale effects upon cavitation and flashing in free and submerged jets. *Trans. ASME* D: *J. Basic Engng* **88**, 525–532.

MICHALKE, A. & FUCHS, H. V. 1975 On turbulence and noise of an axisymmetric shear flow. *J. Fluid Mech.* **70**, 179–205.

OOI, K. K. & KATZ, J. 1980 Flow visualization of cavitation in water jets and nuclei distribution measurements by holography. *Cavitation and Polyphase Flow Forum, ASME Conf., New Orleans.*

OOI, K. K. 1981 Scale effects on cavitation inception in submerged jets. Ph.D. dissertation, California Institute of Technology.

OOI, K. K. & ACOSTA, A. J. 1983 The utilization of specially tailored air bubbles as static pressure sensors in a jet. *Mixing in Turbulent Flows Session, ASME Conf., Houston, Texas.*

PERRY, J. A. & WATMUFF, J. H. 1981 The phase-averaged large scale structures in three-dimensional turbulent wakes. *J. Fluid Mech.* **103**, 33–51.

PETERSON, F. B., DANEL, F., KELLER, A. & LECOFFE, Y. 1975 Determination of bubble and particulate spectra and number density in a water tunnel with three optical techniques. In *Proc. 14th ITTC, Ottawa*, vol. 2, pp. 27–52.

SAMI, S., CARMODY, T. & ROUSE, H. 1967 Jet diffusion in the region of flow establishment. *J. Fluid Mech.* **27**, 231–252.

WINANT, C. D. & BROWAND, F. K. 1974 Vortex pairing: mechanism of turbulent mixing layer growth at moderate Reynolds number. *J. Fluid Mech.* **63**, 237–255.